Surface & Coatings Technology 258 (2014) 310–319

Contents lists available at ScienceDirect

Surface & Coatings Technology

journal homepage: www.elsevier.com/locate/surfcoat

Preparation of superhydrophobic polyimide films modified with organosilicasol as effective anticorrosion coatings

Teng-Yuan Lo, Yi-Chia Huang, Yi-Nan Hsiao, Chuen-Guang Chao, Wha-Tzong Whang *

Department of Materials Science and Engineering, National Chiao Tung University, Hsinchu 30049,Taiwan

ARTICLE INFO

Article history:
Received 16 June 2014
Accepted in revised form 5 September 2014
Available online 16 September 2014

Keywords:
Superhydrophobicity
Surface roughness
Contact angle
Silylation
Fluoro-organosilicasol
Anticorrosion

ABSTRACT

In this study we prepared superhydrophobic polyimide (PI) hybrid coatings for anticorrosion application by adjusting their surface roughness and surface composition through spray-coating with silylated perfluoroalkylsilane-modified organosilicasol (silylated fluoro-organosilicasol), which increased the surface hydrophobicity. After silylation with 1,1,1,3,3,3-hexamethyldisilazane (HMDS), the silylated fluoro-organosilicasol further transformed the PI surface into a superhydrophobic state with a static water contact angle of greater than 160° and a low hysteresis of 10°. We examined the mechanism behind the enhancement in superhydrophobicity through analyses of the surface topology and chemical composition of the films, using Fourier transform infrared spectroscopy (FTIR), scanning electron microscopy (SEM), atomic force microscopy (AFM), and electron spectroscopy for chemical analysis (ESCA). These analyses suggested that both surface roughness and silylation of the fluoro-organosilicasol making more CF_2 groups on the outmost surface rendered the surface hydrophobicity. The anticorrosion properties of these superhydrophobic coatings were also examined through Tafel measurement. These PI hybrid coatings demonstrated lower corrosion current density and nobler corrosion potential and higher polarization resistance. The enhancement in anticorrosion performance was believed to be contributed from the superhydrophobicity and dual barrier protection from the fully-covered fluoro-organosilicasol, insulating the metal from corrosive species in the medium. This superhydrophobic coating technique with good stability guaranteed better corrosion protection and also has great potential for application to other polymeric films.

1. Introduction

Polyimide (PI) is already a widely used flexible polymer exhibiting good thermal, chemical, and mechanical properties [1]. PIs are also utilized as stable organic coatings for anticorrosion purposes due to the advantages listed above. However, the limitation of PI as an organic coating lies in the water absorption [2], which is a drawback for its use in coating for anticorrosion. The adoption of fluorine-containing monomers can enhance the hydrophobicity of PI [3] but superhydrophobicity cannot be simply achieved with monomer substitution since the surfaces have to be rough. The major limitation toward achieving superhydrophobicity of PI surfaces, however, lies in its flatness and poor workability after imidization. According to previous studies, a flat surface presenting regularly aligned closest-hexagonal-packed CF_3 groups can achieve a water contact angle of only 120° [4]. To prepare superhydrophobic PI, appropriate control of the surface roughness is the critical factor toward enhancing hydrophobicity, according to the Wenzel and Cassie equations, which both describe the wetting behavior of rough surfaces [5].

Although many approaches have been developed for the fabrication of superhydrophobic surfaces, including electrospinning [6], etching [7], plasma treatment [8,9], chemical vapor deposition (CVD) [10,11], addition of a sublimation material [12,13], molding [14,15], electrodeposition [16], and sol–gel processing [17–20], the modification techniques to create rough structures on PI surfaces remain a challenge. Recently, nanoparticles (NPs) have become popular modifying agents for controlling surface roughness [21]. With their precise size control, tunable surface chemistry, and high processability through spin- or dip-coating, NPs appear to be excellent materials for producing superhydrophobic coatings [22–30]. These techniques for preparing superhydrophobic PI coating could be promising in application for anti-corrosion and anti-contamination use in harsh environment [31–33].

In this paper, we describe the endowing of superhydrophobicity onto the surface of PI films for anticorrosion using a simple method: spray-coating with an excellent anchor on the surface. Here, we employed fluoroalkylsilane-modified organosilicasol (DMAc-ST), which is spherical colloidal silica mono-dispersed in the organic solvent N,N-Dimethyl acetamide with particular particle size, to create rough features on the surfaces of soluble PI. We modified the organosilicasol DMAc-ST in a two-step process: first with fluoroalkylsilane (tridecafluoro-1,1,2,2-tetrahydrooctyl-1-triethoxylsilane, F8261) to hydrophobize DMAc-ST [29], then with the silylation agent 1,1,1,3,3,3-hexamethyldisilazane

* Corresponding author: Tel.: +886 3 5131873; fax: +886 3 5724727.
E-mail address: wtwhang@mail.nctu.edu.tw (W.-T. Whang).

http://dx.doi.org/10.1016/j.surfcoat.2014.09.008
0257-8972/

(HMDS) further to remove residual SiOH groups [30]. After surface modification, we spray-coated the silylated fluoro-organosilicasol onto the PI surfaces. Through this simple process, we could anchor the sprayed silylated fluoro-organosilicasol onto the film's surface to provide suitably rough surface features, thereby enhancing the hydrophobicity and minimizing contact angle hysteresis. Furthermore, we believe the combination of silylated fluoro-organosilicasol and PI can provide good water repellency and dual barrier protection for anticorrosion on steel. Using contact angle measurements, scanning electron microscopy (SEM), atomic force microscopy (AFM), Fourier transform infrared (FTIR) spectroscopy, and electron spectroscopy for chemical analysis (ESCA) and Tafel polarization curves for corrosion measurement, we characterized the mechanism of superhydrophobicity enhancement and the anticorrosion behaviors of the PI hybrid coatings.

2. Experimental

2.1. Materials

2,2′-Bis(3,4-dicarboxyphenyl) hexafluoropropane dianhydride (6FDA) and 2,2-Bis [4-(4′-aminophenoxy)phenyl] hexafluoropropane (6FBAPP) were purchased from ChrisKev. Organosilicasol (DMAc-ST ZL, 20 wt% spherical colloidal silica mono-dispersed in N,N-dimethylacetamide (DMAc); particle size: 70–100 nm; Nissan Chemical), tridecafluoro-1,1,2,2-tetrahydrooctyl-1-triethoxylsilane (F8261, 95%+; Alfa Aesar), 1,1,1,3,3,3-hexamethyldisilazane (HMDS) (98%; ACROS), hydrochloric acid (HCl, 37%; Merck), N,N-dimethylacetamide (DMAc, 99%+; Tedia) and toluene (99%+; Tedia) were stored in desiccators and used as received. Stainless steel 304 (SS304) plates with 0.1 mm thickness were purchased from a local supplier and mechanically abraded with different grades of emery paper and then polished with 0.3 mm alumina powder. The polished SS304 plates were washed with distilled water and ethanol.

2.2. Synthesis of PI-coated SS304 film

6FBAPP with equal mole numbers to 6FDA was first added in three portions to DMAc solvent in a 250-mL three-neck round-bottomed flask equipped with a mechanical stirrer and N_2 inlet. After the diamine had completely dissolved, an equal number of moles of 6FDA was added, in three portions, to the solution. After the 6FDA had completely dissolved in the reaction mixture, the solution was further stirred for 2 h to obtain a higher molecular weight of poly(amic acid). This poly(amic acid) solution was then coated onto SS304 plates and subjected to thermal imidization sequentially at 100, 150, 200 °C for 1 h each. Bare SS304 and PI-coated SS304 plates were cut into square films with 2.5 × 2.5 cm^2 per piece to undergo further measurement.

2.3. Synthesis of silylated fluoro-organosilicasol

DMAc-ST was diluted to 0.5 wt% by adding DMAc solvent and then F8261 (an equal weight to the DMAc-ST solid content) was added slowly to the solution. The DMAc solution was stirred at 100 °C for 24 h to form fluoro-organosilicasol. The pH of this solution was then adjusted to 1.2 by adding concentrated HCl (37%). HMDS was slowly added dropwise to the acidified solution to silylate the fluoro-organosilicasol; this reaction took place in an ultrasound bath over 12 h at room temperature. The supernatant liquid was then removed through baking at 160 °C for 6 h and the silylated fluoro-organosilicasol was collected and dried. The nonsilylated fluoro-organosilicasol was also subjected to the same procedure for the sake of comparison.

2.4. Preparation of superhydrophobic PI-coated films

Silylated fluoro-organosilicasol and fluoro-organosilicasol were separately dispersed in DMAc and toluene (1:1) so that the solid content was 5 wt% in each solution. The solutions containing the silylated and nonsilylated fluoro-organosilicasols were separately spray-coated (one, two, or four cycles with constant time per cycle) onto several PI-coated SS304 films; the volume of each spray was fixed at 0.01 mL over an area of 2.5 × 2.5 cm^2. Spray-coating was performed using a spray pistol and N_2 gas under a constant pressure (50 psi). PI coating films modified with the silylated and nonsilylated fluoro-organosilicasols are denoted herein as PI-FH_x and PI-F_x, respectively, where x represents the number of sprays. These modified PI-coated SS304 films were baked at 50 °C for 10 min and then at 160 °C for 2 h to ensure that no solvent remained. The baking process also served to anchor the particles to the surface.

2.5. Characterization

The surface wettability of the samples was determined using a contact angle meter by measuring the water contact angle of one drop (10 μL) of deionized water at room temperature. Three measurements were performed for each sample to evaluate the average static contact angle (θ) after 5 s. Films were tilted at 10° to record the dynamic motions of the water droplets on the sample surfaces. Contact angle hysteresis was investigated by measuring advancing and receding contact angle through tilting experiment. Surface morphologies and particle distributions were investigated using a thermal field emission scanning electron microscope (JEOL JSM-6500 F). An atomic force microscope (Innova Scanning Probe Microscope) was used to derive surface roughness profiles. All AFM measurements of the PI, PI-F_x, and PI-FH_x series were performed in the tapping mode in a dry environment at room temperature over a sampling area of 5 × 5 μm^2. The images had a resolution of 512 × 512 pixels and were acquired at a scanning rate of approximately 0.5 Hz. The images obtained were processed using diSPMLab software (Veeco). FTIR spectra of fluoro-organosilicasols prepared with and without HMDS treatment were recorded using a PerkinElmer Spectrum 100 Optica spectrometer. The surface chemistry of the PI, PI-F_x, and PI-FH_x series was characterized through ESCA (Ulvac-PHI PHI 1600) with a 15 kV Al/Mg X-ray source and the Mg K_α emission at 1253.6 eV. A single-scan spectrum (0–1100 eV) and narrow scans for C 1 s (280–300 eV) were recorded for each sample with pass energies of 1 and 0.1 eV, respectively. The background was subtracted using the Shirley formula; deconvolution was performed by fitting the spectra to multiple peaks, each being a Gaussian function; the charge effect was compensated by setting the binding energy of aromatic C atoms, not linked to O or N atoms, at 285.0 eV. Cross-cut tests were used to determine the adhesion of the surface coating. Specimens were cross-cut to create 100 squares pieces within 1x1 cm^2 and 3 M 600 tape was applied over the cut. Then the tape was pulled

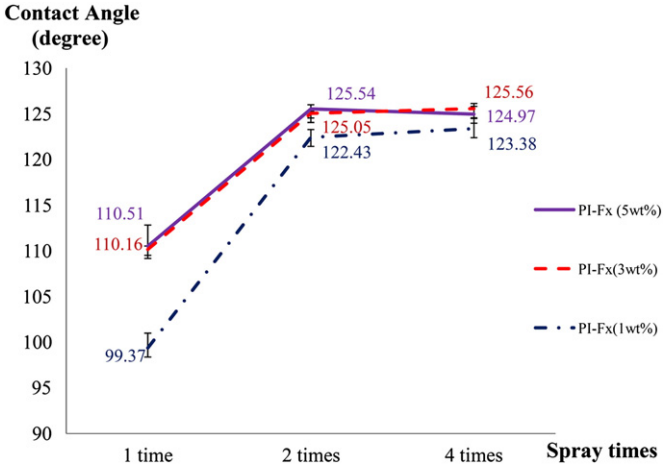

Fig. 1. Contact angle curves of PI-F_x films coated with different concentrations of the modified particles and subjected to different numbers (one, two, or four) of spray coatings.

Table 1
Static, advancing, and receding contact angles[a] of films of unmodified PI and PI-F_x (coated with organosilicasol at concentrations of 1, 3, and 5 wt%).

contact angle (degree) / Spray cycles	Unmodified	PI-F_x (1 wt%)	PI-F_x (3 wt%)	PI-F_x (5 wt%)	Advancing contact angle (5 wt%)	Receding contact angle (5 wt%)
0	94.98 ± 0.09°				98.67 ± 1.54°	32.84 ± 0.33°
1		99.37 ± 1.62°	110.16 ± 2.66°	110.51 ± 0.02°	132.46 ± 2.78°	64.59 ± 1.12°
2		122.43 ± 0.85°	125.05 ± 0.21°	125.54 ± 0.45°	135.01 ± 3.04°	55.31 ± 0.79°
4		123.38 ± 1.11°	125.56 ± 0.26°	124.97 ± 1.16°	133.47 ± 2.14°	52.46 ± 1.32°

[a] Values was expressed as Mean values ± SD.

off from samples rapidly to see how much area left on the specimens. To investigate the coating durability in salt water, test samples were also soaked in 3.5 wt% NaCl aqueous solution for 7 days before adhesion test.

The electrochemical corrosion was measured by using a Solartron SI 1287. The measurements were made in a three-electrode electrochemical cell; platinum sheet electrode and saturated calomel electrode (SCE) were used as counter and reference electrodes, respectively. The electrochemical test was conducted in 3.5 wt% NaCl aqueous solution at room temperature. Corrosion potential (E_{corr}) was recorded via the open circuit potential (OCP) method at the equilibrium state of the system. The Tafel plots were obtained by scanning from −0.2 V versus E_{corr} to +0.2 V versus E_{corr} at a scan rate of 10 mV/min. The corrosion current density (i_{corr}) was determined by extrapolation of a tangent line along the linear part of the cathodic and anodic curve through E_{corr}. We also inferred polarization resistance (R_p) and corrosion rate from i_{corr}. The R_p can be obtained as follows:

$$R_p = \frac{\Delta E}{\Delta I} = \frac{\beta_a \cdot \beta_c}{2.303 \cdot i_{corr}(\beta_a + \beta_c)} \quad (1)$$

where β_a and β_c are the anodic and cathodic Tafel slope, respectively. The corrosion rate was calculated as follows:

$$\text{corrosion rate (mm/yr)} = \frac{3270 \cdot i_{corr}\left(A/cm^2\right) \cdot EW}{D} \quad (2)$$

where 3270 is the conversion factor for corrosion rate in mm/yr and i_{corr} in A/cm^2; D is the specimen density in g/cm^3 (8.03 g/cm^3 for SS304); EW is the specimen equivalent weight in grams (26.966 g/eq for SS304). The electrochemical impedance spectroscopy (EIS) measurements were performed by using a Solartron SI 1255B at OCP with 10 mV amplitude in an applied frequency ranged from 100 KHz down to 0.01 Hz.

3. Results and discussion

3.1. Contact angles and FTIR spectra

To transform PI surfaces into superhydrophobic ones, we designed a coating method involving the spraying of fluoro-organosilicasol NPs onto the PI surfaces. Fig. 1 presents the effects of spray cycles on the water/surface contact angle of the unmodified PI and PI-F_x films. The water contact angle data are listed in Table 1. Although fluoro-organosilicasol could enhance the water/surface contact angle of PI-F_x up to 125.56°, contact angles level off even when increasing the concentration of the coating particles or the spray cycles.

We used the FTIR spectrometer to investigate this phenomenon. The FTIR spectrum of fluoro-organosilicasol (Fig. 2) features a mid-intensity band in the range 3100–3700 cm^{-1}, due to OH stretching vibrations with inter- and/or intramolecular hydrogen bonding, suggesting that a significant number of OH groups appeared on the fluoro-organosilicasol. Obviously, only a fraction of the OH groups of the organosilicasol reacted with F8261 and many OH groups remained on the organosilicasol regardless of the reaction conditions. The residual OH groups offset the enhancement in hydrophobicity and become hindrances to superhydrophobicity. Therefore, we added HMDS to reduce the surface OH groups and upgraded the PI surface to superhydrophobic ones. The FTIR spectrum of the silylated fluoro-organosilicasol is also displayed in Fig. 2. The spectra of both the fluoro-organosilicasol and the silylated fluoro-organosilicasol exhibit the same asymmetric SiOSi stretching band near 1100 cm^{-1} and the same symmetric SiOSi stretching bands near 805 and 474 cm^{-1}. However, the 3100–3700 cm^{-1} broad band of OH groups in fluoro-organosilicasol was absent in the silylated fluoro-organosilicasol. On the other hand, SiMe bands near 1260 cm^{-1} and an additional asymmetric SiOSi stretching peak near 1120 cm^{-1} were present in the spectrum of the silylated fluoro-organosilicasol. The absent signals of OH groups and the new present bands of $SiMe_3$ and SiOSi groups confirmed that silylation had effectively transformed the SiOH groups into $SiOSiMe_3$ units.

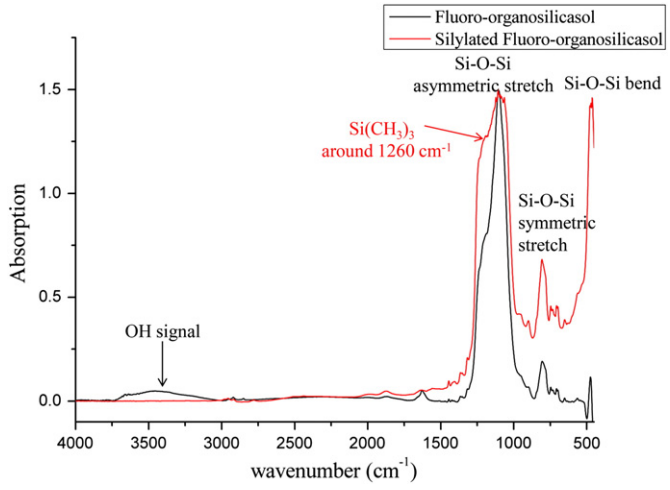

Fig. 2. FTIR spectra of fluoro-organosilicasols prepared with and without HMDS-mediated silylation.

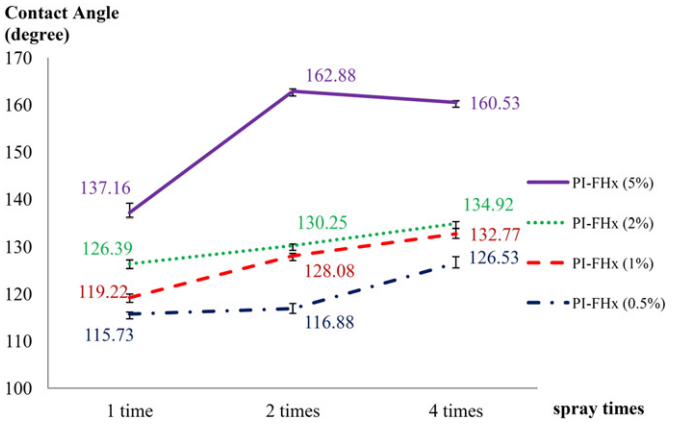

Fig. 3. Contact angle curves of PI-FH_x films coated with different concentrations of the modified particles and subjected to different numbers (one, two, or four) of spray coatings.

Table 2
Static, advancing, and receding contact angles[a] of films of unmodified PI and PI-FH_x (coated with organosilicasol at a concentration of 0.5, 1, 2, and 5 wt%) and of the film of PI-FH_2 (coated at 5 wt%) after ultrasonication treatment for 10 min.

contact angle (degree) / Spray coating cycles	PI-FH_x (0.5 wt%)	PI-FH_x (1 wt%)	PI-FH_x (2 wt%)	PI-FH_x (5 wt%)	Advancing contact angle (5 wt%)	Receding contact angle (5 wt%)
1	115.73 ± 0.41°	119.22 ± 0.76°	126.39 ± 0.82°	137.16 ± 1.97°	140.19 ± 3.44°	116.97 ± 1.65°
2	116.88 ± 1.09°	128.08 ± 0.52°	130.25 ± 0.33°	162.88 ± 0.52°	167.34 ± 2.87°	162.66 ± 2.33°
4	126.53 ± 1.38°	132.77 ± 1.13°	134.92 ± 0.43°	160.53 ± 0.35°	168.82 ± 2.66°	164.77 ± 2.78°
PI-FH_2(5 wt%) ultrasonication			156.63 ± 0.49°			

[a] Values was expressed as mean values ± SD.

Fig. 3 presents the surface water contact angles of PI-FH_x versus coating spray cycles. PI-FH_x are the PI films surface-modified with the HMDS-treated fluoro-organosilicasol at different concentrations. Table 2 lists the average values and deviations. The PI-FH_x species provided contact angles higher than those of the corresponding PI-F_x species; accordingly, the surface hydrophobicity was greatly enhanced after silylation treatment on fluoro-organosilicasol. In PI-FH_x series, the surface water contact angles increased with the particle concentration and spray cycles as well, except when applying the 5 wt% coating solution. When spraying with 5 wt% solution, the water contact angles leveled off, and were 162.88 ± 0.52, and 160.53 ± 0.35° for PI-FH_2, and PI-FH_4, respectively. The water contact angles of the PI-FH_x systems seemed to level off when spray cycles $x \geqq 2$, with no apparent increase upon increasing the cycle of spray coatings. The similar leveling-off situation was also observed on PI-F_x films (Fig. 1). Therefore, we inferred that this PI could display superhydrophobicity after spray-coating its surface twice with the 5 wt% solution. Accordingly, our following discussions are focused on the samples in both the PI-F_x and PI-FH_x series that had been treated with the 5 wt% solution.

Fig. 4 displays images of water droplets on films of PI, PI-F_x, and PI-FH_x. The PI-F_2 and PI-FH_x surfaces were clearly more hydrophobic than unmodified PI. Compared to the PI-F_2 shown in Fig. 4(b), all the PI-FH_x films exhibited greater water repellency. The water droplets adopted spherical shapes on the PI-FH_2 film in Fig. 4(d), confirming

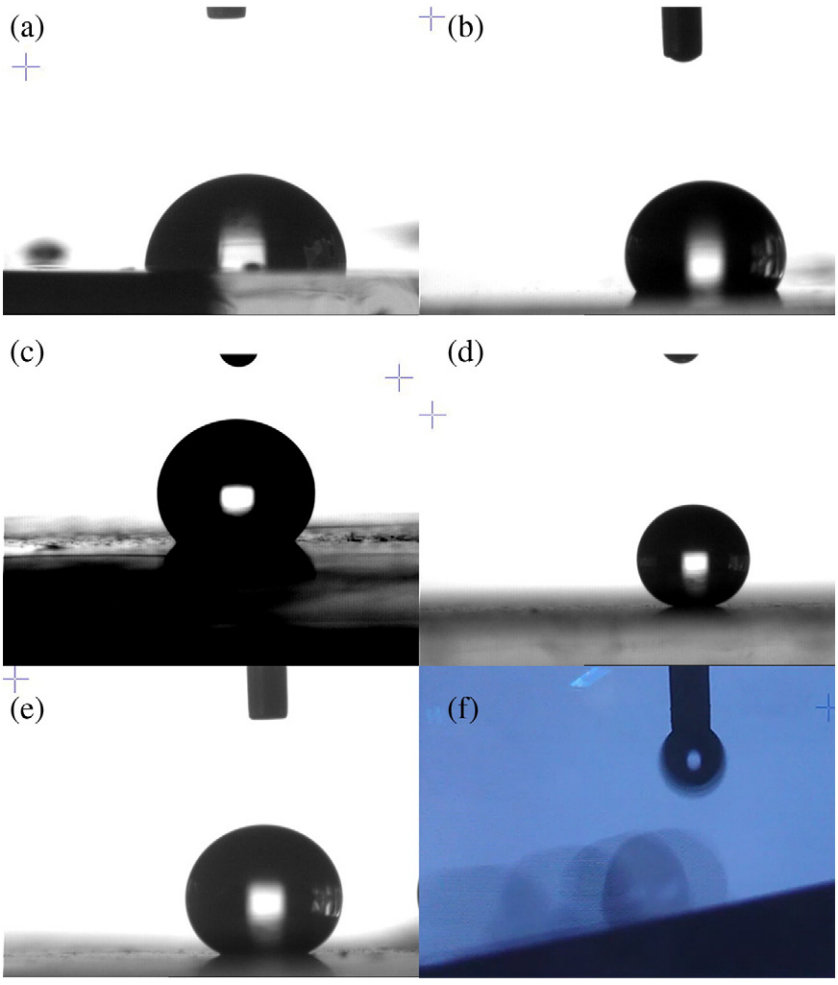

Fig. 4. Images of water droplets on the surfaces of (a) PI, (b) PI-F_2, (c) PI-FH_1, (d) PI-FH_2, and (e) PI-FH_2 after 10 min ultrasonication; (f) video screenshot of the rolling motion of water droplets on the PI-FH_2 surface tilted by approximately 10°.

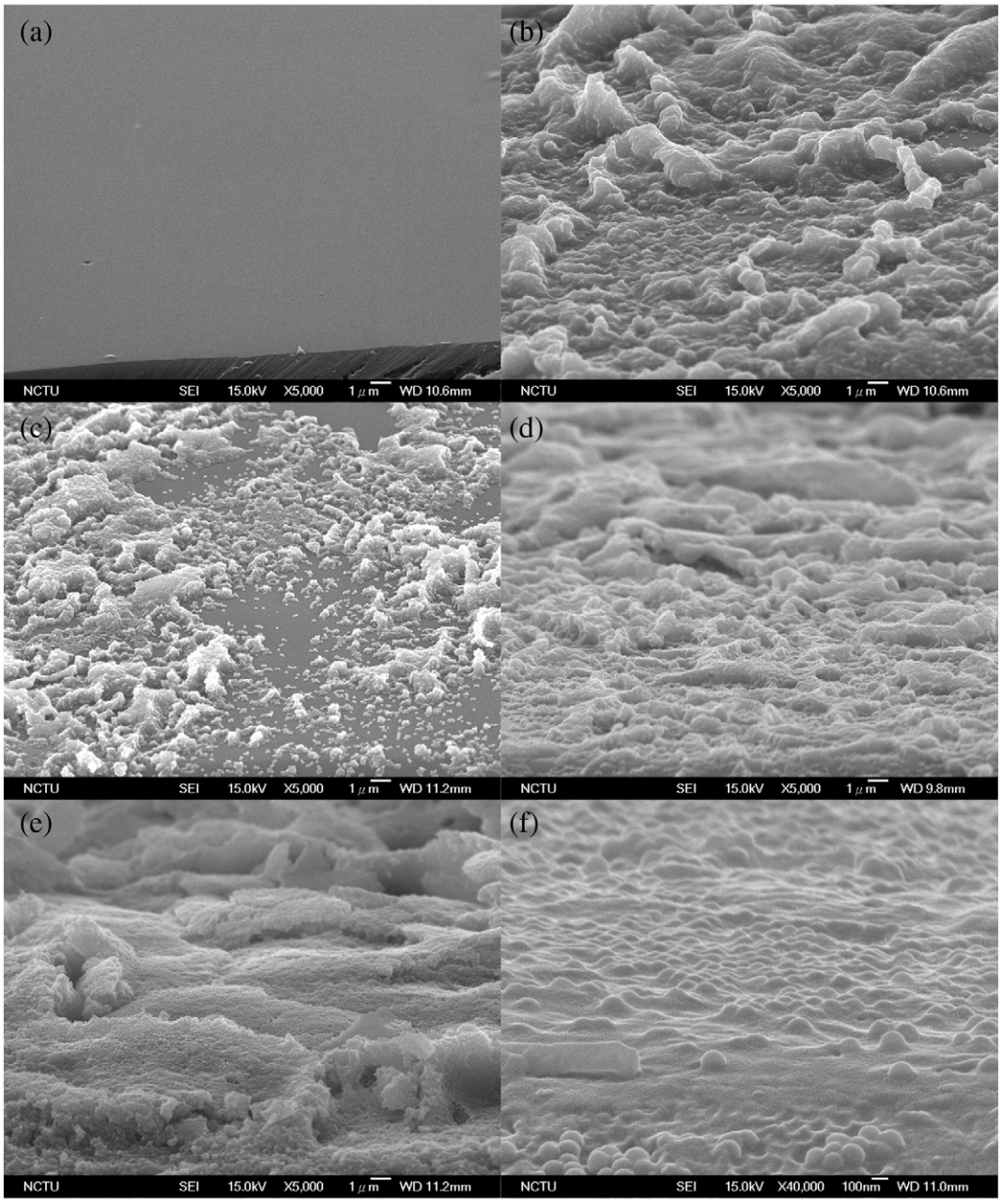

Fig. 5. Tilted top-view SEM images of (a) unmodified PI, (b) PI-F_2, (c) PI-FH_1, (d) PI-FH_2, and (e) PI-FH_4; (f) particle-matrix interfacial image of PI-FH_1.

the much greater water repellency on the silylation-modified surfaces. After 10 min of ultrasonication treatment in water, the PI-FH_2 film retained its superhydrophobicity, with a water contact angle of $156.63 \pm 0.49°$ [Fig. 4(e)], suggesting excellent surface anchoring stability. Fig. 4(f) displays a video screenshot of water droplets readily rolling down the PI-FH_2 surface on a slope of 10°. According to Table 2, PI-FH_2 and PI-FH_4 both had low contact angle hysteresis (<10°). In the same tests performed on the PI-F_x species shown in Table 1, the contact angle hysteresis of PI-F_x series are higher than that of PI-FH_x, showing water droplets stuck strongly to the surfaces of PI-F_x films. Previous reports have suggested that rough surfaces following the Cassie equation exhibit lower hysteresis than do those following the Wenzel equation, which considers water droplets as being immersed into grooves having rough features and are, thus, sticky [5,34]. Based on the results of advancing and receding contact angles, we suggested that the surface features of the superhydrophobic PI-FH_x films ($x \geq 2$) followed the Cassie equation, in which the droplets reside on top of the surface structures. The characteristics and mechanisms of the water contact behaviors were verified with the following measurements: SEM, AFM, and ESCA.

Table 3
Roughness parameters – R_q (root-mean-square roughness), R_a (average roughness), and R_{max} (maximum peak-to-valley height) – of films of PI, PI-F_x, and PI-FH_x.

	R_q (nm)	R_a (nm)	R_{max} (nm)
PI	0.596	0.484	6.20
PI-F_1	137	101	1160
PI-F_2	189	145	1430
PI-F_4	313	261	1710
PI-FH_1	145	117	972
PI-FH_2	189	143	1300
PI-FH_4	331	265	1900

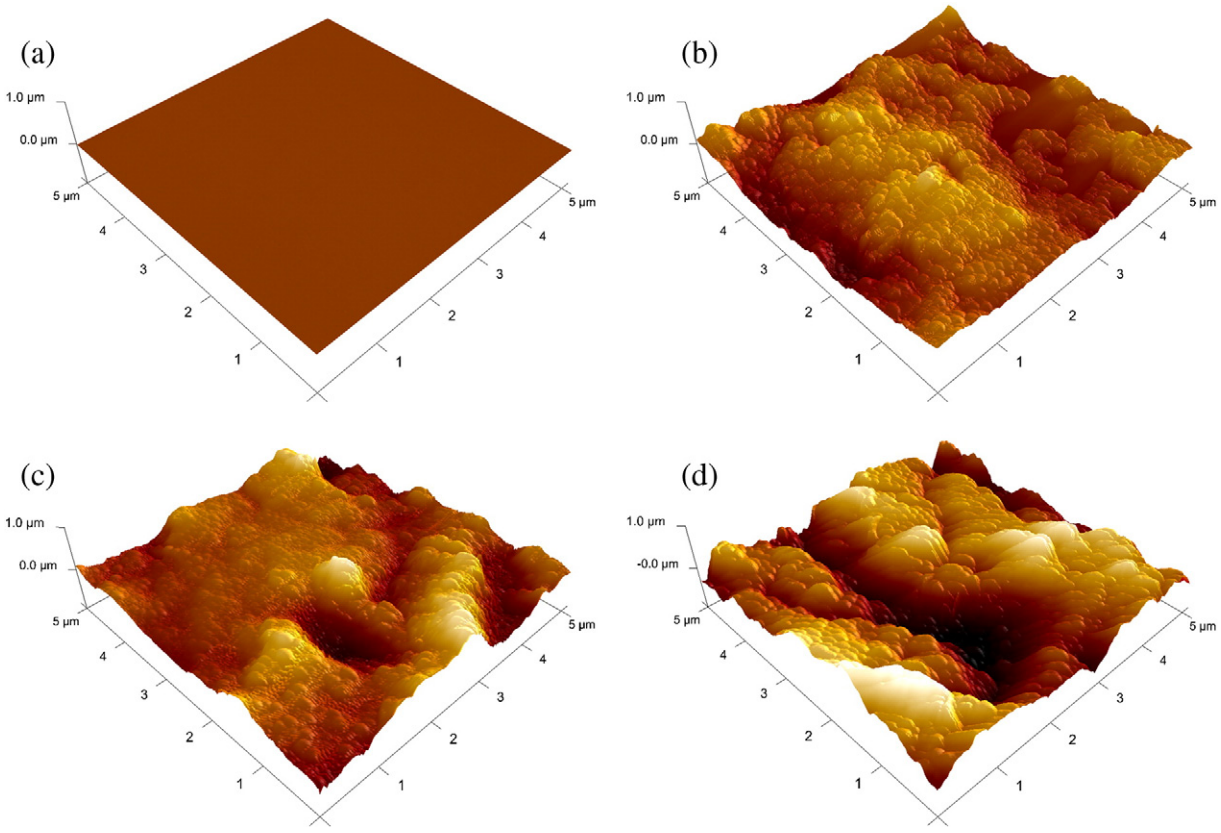

Fig. 6. 3-D AFM topology images of (a) PI, (b) PI-FH_1, (c) PI-FH_2, and (d) PI-FH_4.

3.2. SEM

Fig. 5 presents top-view SEM images of films of pristine PI, PI-F_2, and PI-FH_x systems with different coatings, revealing the surface topologies and particle distributions on the PI surfaces. In Fig. 5(a), unmodified PI displays the smooth surface. PI-F_2 appears to have a rough surface, as shown in Fig. 5(b). Fig. 5(c) reveals the uneven surface morphology of PI-FH_1; the silylated fluoro-organosilicasol appeared to be randomly size-distributed on the surface of PI-FH_1, with particles only partially covering the surface. In Fig. 5(d), we observed the PI-FH_2 surface fully covered by the silylated fluoro-organosilicasol, with a morphology similar to that of PI-F_2 in Fig. 5(b), but with the particle clusters somewhat larger and approaching a more uniform size. Thus, spray-coating twice resulted in excellent surface coverage. When we sprayed the film four cycles, the silicasol particles on the surface of PI-FH_4 aggregated to form a coarser and more regular morphology [Fig. 5(e)]. These results indicate that a greater number of coatings causes the particles to aggregate into larger clusters, creating greater surface roughness on the PI-FH_2 and PI-FH_4 films and, thereby, more valley-like structures on the surfaces. Such valley-like features may trap air within the structure when a water droplet is placed on its surface. According to the Cassie equation, a section of air at the contact interface is essential to achieve superhydrophobicity. Fig. 5(f) presents a tilted top-view image of the PI-FH_1 film at higher magnification. We observe that the deposition of the first layer of particles on the PI surfaces caused the lower portions of the particles to be embedded into the PI matrix, forming a firm layer that functioned as a stable base upon which more particles could overlap. The immersion depth appeared to be about half the particle diameter, according to Fig. 5(f). In the spray process, the dispersed particles were brought to the surfaces in a co-solvent of DMAc and toluene. DMAc swelled the PI surfaces, causing the particles to immerse partly into the PI surfaces. During the baking process, the residual solvent molecules evaporated and, thus, the particles were embedded with tight anchoring to the surfaces. Thus, baking served the function of stabilizing the aggregates. The SEM images provide a strong rationale for why the modified PI films exhibited good sustainability after treatment in the ultrasonication bath.

3.3. AFM

We used AFM to scan the surface topologies of the PI, PI-F_x, and PI-FH_x films over an area of 5 × 5 μm^2. Table 3 lists the values of R_q (root-mean-square roughness), R_a (average roughness), and R_{max} (maximum peak-to-valley height) of these species. Fig. 6 presents the three-dimensional (3-D) AFM surface topologies of the PI and PI-FH_x films. According to Fig. 6(a) and Table 3, the PI matrix was quite flat, with values of R_q and R_a both below 1 nm. For the modified PI systems, the surface topology became rougher upon increasing the number of spray cycles [cf. Fig. 6(b)–(d)]. The particles formed larger clusters and the surface morphologies transformed from numerous hills to a mountains-and-valleys topology, consistent with the SEM data. The data of Table 3 reveals that PI-F_1 and PI-FH_1 have similar R_q (137 vs 145 nm) and R_a (101 vs 117 nm). With a number of coatings, R_q and R_a of both series also remained close to each other. The surface

Table 4
Surface elemental compositions of PI, PI-F_2, and the PI-FH_x series, determined through ESCA.

	C 1 s	N 1 s	O 1 s	F 1 s	Si 2p
PI	70.20%	2.57%	9.30%	17.93%	0.00%
PI-F_2	20.56%	0.00%	33.89%	22.64%	22.92%
PI-FH_1	33.66%	0.00%	14.29%	41.37%	10.67%
PI-FH_2	33.16%	0.00%	14.17%	41.94%	10.73%
PI-FH_4	34.17%	0.04%	14.29%	41.49%	10.01%

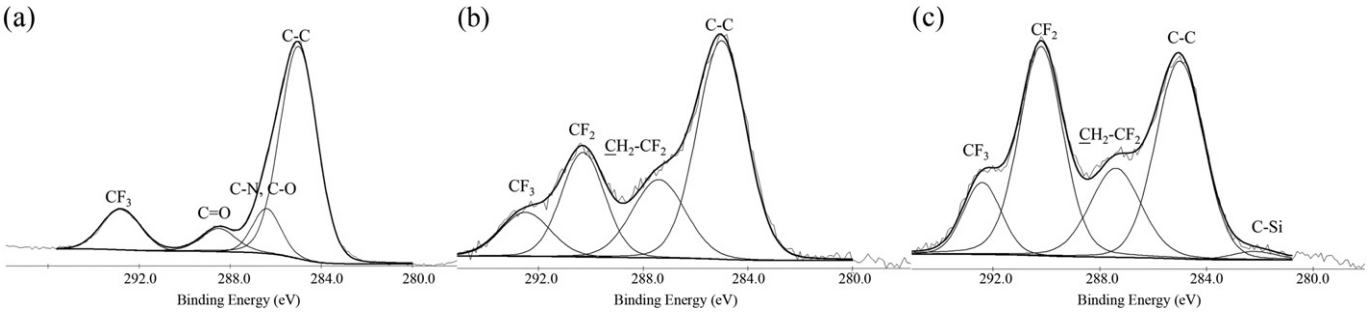

Fig. 7. Deconvolution of the C 1 s X-ray photoelectron spectra of (a) PI, (b) PI-F_2, and (c) PI-FH_2.

Table 5
Proportional area of each bonding peak in the deconvoluted C 1 s X-ray photoelectron spectra of PI, PI-F_2, and PI-FH_2.

	C-Si	C-C	C-N,C-O	C = O	CH_2-CF_2	CF_2	CF_3
PI	0%	68.34%	11.00%	7.67%	0%	0%	12.98%
PI-F_2	0%	49.51%	0%	0%	19.35%	21.01%	10.12%
PI-FH_2	1.43%	35.30%	0%	0%	17.65%	35.55%	10.06%

roughness of both PI series increased with the number of spray coatings. PI-F_x and PI-FH_x possessed similar roughness parameters and topologies because of the same NP-base. The only difference lay in the surface OH groups on PI-F_x transformed into $OSiMe_3$ on PI-FH_x.

Although the surface roughnesses of both series of films increased upon increasing the number of spray coatings, their contact angles increased only up to twice spray coating and leveled off thereafter. Thus, the surface roughness promoted the surface water contact angle to a certain extent, but further boosting required another mechanism. Considering the superhydrophobicity and low contact angle hysteresis exhibited in PI-FH_2 and PI-FH_4, we believed that at least twice spray cycles can create rough surfaces rendering high air-trapping capacity within water/surface interface. The similar surface morphologies of PI-F_x and PI-FH_x, however, leaded to different water/surface contact behaviors. The greater superhydrophobicity of the PI-FH_x systems was presumably due to a factor other than the surface roughness alone; this factor was the silylation of the fluoro-organosilicasol, a process that resulted in a change to the chemical environment of the particle surface.

3.4. ESCA

We used ESCA to analyze the surface elemental composition and nature of the chemical bonding within the unmodified PI and modified PI-F_x and PI-FH_x films. Table 4 lists the surface elemental compositions of these films. The pristine fluorine-containing PI presented 17.93 atom% of fluorine on its surface. After coating with the fluoro-organosilicasol, the PI-F_2 film surface presented a slightly higher F content of 22.64 atom%—far less than the theoretical value of approximately 46 atom% expected based on the presence of long perfluoroalkyl chains of the fluoro-organosilicasol on the surface. This observation implies that the perfluoroalkyl chains were not fully stretched out of the surface because of OH groups on the particle surface. When the surfaces were modified with the trimethylsiloxy groups, there was a significant advancement in F atom%, rising to 41–42 atom%, much closer to the theoretical value. Clearly, silylation changed the surface chemical environment to be more hydrophobic, which favored the perfluoroalkyl chains stretching on the surface. The surface compositions of PI-FH_x films were almost identical. Thus, increasing the spray cycles affected only the stacking of particles, not the surface chemical environment of the films.

In addition to the great differences in the F atom compositions of the PI-F_2 and PI-FH_x species, their C atom contents were 20.56 and 33.66 atom%, respectively, their O atom contents were 33.89 and 14.29 atom%, respectively, and their Si atoms contents were 22.92 and 10.67 atom%, respectively. The PI-F_2 surface featured a lower content of C atoms and much higher contents of O and Si atoms than did the PI-FH_x surfaces, hinting that much more O- and Si-related groups extended from the PI-F_2 surface. From these FTIR spectroscopic data, we conclude that the O- and Si-related groups must be SiOH units. We examined the deconvolution curves of the C 1 s signal spectra of PI, PI-F_2, and PI-FH_2 (Fig. 7) to further investigate the surface environments in more detail. The C 1 s spectrum of pristine PI could be resolved into several components, namely for CC (285 eV), COC (286.4 eV), CN (286.4 eV), C = O (288.5 eV), and CF_3 (292.8 eV) groups, all of which appear in the main structure of pristine PI. For PI-F_2 in Fig. 7(b), we could deconvolute the C 1 s signals into four components: CC (285 eV), CH_2CF_2 (287.4 eV), CF_2 (290.3 eV), and CF_3 (292.5 eV) groups. The C 1 s signal of PI-FH_2 [Fig. 7(c)] possessed the same components as those of PI-F_2 as well as

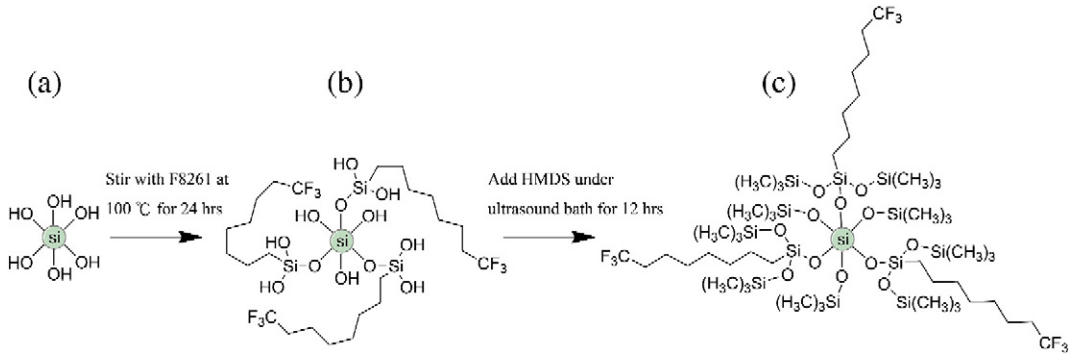

Fig. 8. Schematic representation of the conformations of the surface groups of the organosilicasol (a) without perfluoroalkylation, (b) after perfluoroalkylation with F8261, and (c) after sequential perfluoroalkylation and HMDS-mediated silylation.

an additional peak for CSi groups (282.2 eV), which arose from $SiOSiMe_3$ units after silylation. In Fig. 7(b) and (c), all of these deconvoluted components, except for that for the CSi groups, were contributed by the perfluoroalkyl chains of F8261 [35]. The peaks representing PI disappeared almost completely from the film surface, revealing the good covering efficiency of the modified particles. Table 5 lists the proportions of each bonding peak in the deconvoluted C 1 s spectra from the ESCA of PI, PI-F_2, and PI-FH_2. Relative to PI-F_2, PI-FH_2 exhibited a higher proportion of CF_2 groups. The peak area proportion of CF_2 groups on PI-FH_2 was 35.65 atom%, close to the proportion found in F8261 monolayers [36], and significantly greater than that (21.01 atom%) on PI-F_2. In contrast, the PI-FH_x and PI-F_2 surfaces both featured approximately the same proportion of CF_3 groups (ca 10 atom%), arising from the chain end of F8261. These findings indicate that the increase in the proportion of CF_2 groups was primarily responsible for the enhancement of the superhydrophobicity of the PI-FH_2 surface, corresponding to the great increase in intensity of the signal for the CF_2 groups of PI-FH_2. The silylation of fluoro-organosilicasol not only eliminated the surface OH groups but also rearranged the conformation of the perfluoroalkyl chains by stretching of the perfluoroalkyl chains on the outermost surfaces, thereby modifying the surface environment. According to ESCA data, we infer that the superhydrophobicity of the PI-FH_x species

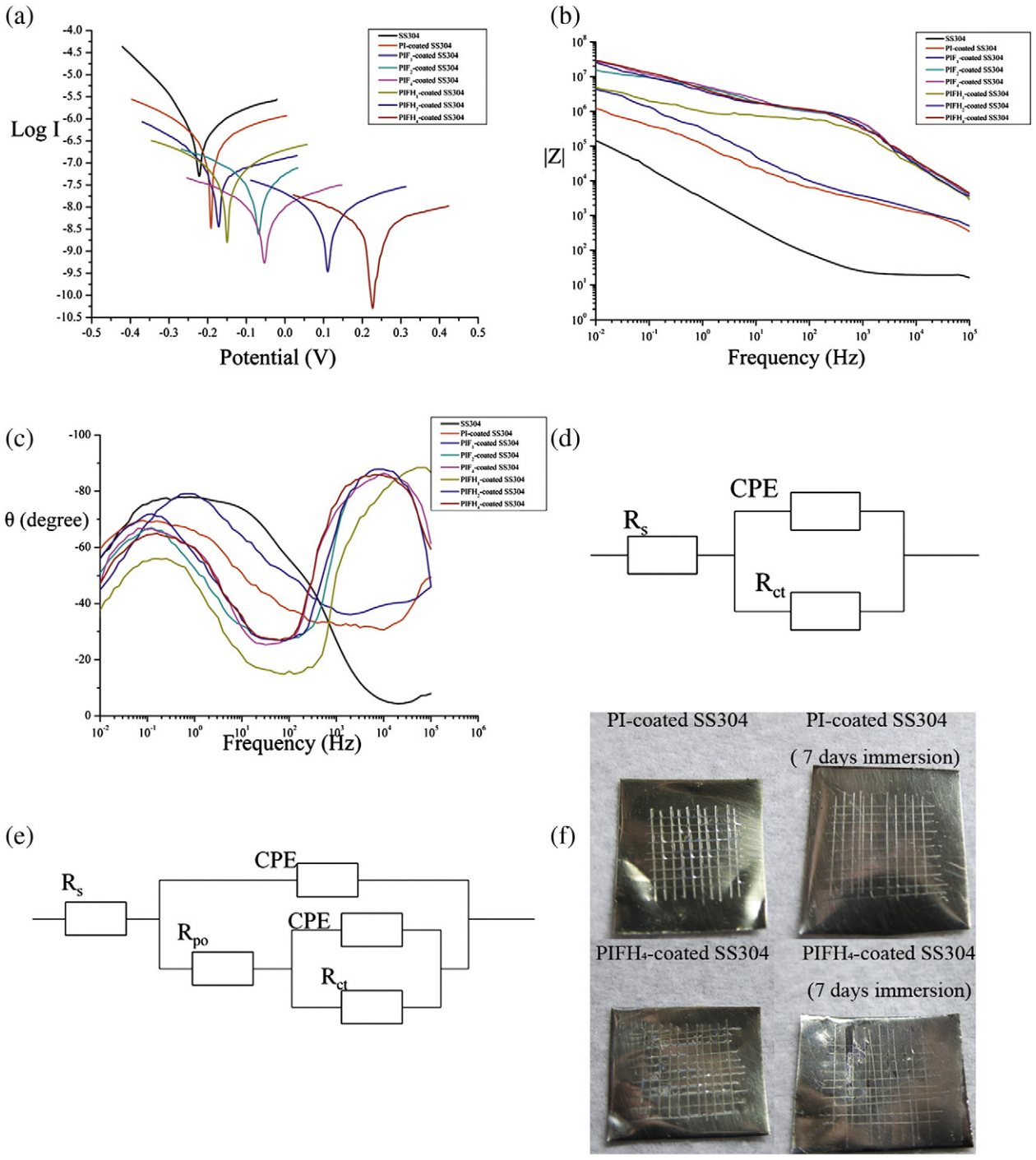

Fig. 9. (a) Potentiodynamic polarization curves and (b-c) Bode plots of SS304, PI-coated SS304, PI-F_x-coated SS304 and PI-FH_x-coated SS304 films exposed to 3.5 wt% NaCl aqueous solution. The equivalent circuit models represent for (d) SS304 and (e) PI-coated SS304 series (including PI-F_x and PI-FH_x). (f) images of PI-coated-SS304 and PIFH4-coated-SS304 films underwent cross-cut test.

Table 6
Electrochemical parameters for inhibition of corrosion of SS304, PI-coated SS304, PI-F_x coated SS304 and PIFH_x-coated SS304 exposed to 3.5 wt% NaCl aqueous solution.

	Corrosion potential (V)	Corrosion current density (A/cm^2)	β_c	β_a	Polarization resistance ($\Omega.cm^2$)	Corrosion rate (mm/yr)	|Z| at 0.01 Hz ($\Omega.cm^2$)
SS304	−0.22	5.690×10^{-7}	0.2106	−0.1131	1.691×10^{5}	6.248×10^{-3}	1.448×10^{5}
PI-coated SS304	−0.191	3.274×10^{-7}	0.2240	−0.1856	1.436×10^{6}	3.595×10^{-3}	1.212×10^{6}
PIF_1-coated SS304	−0.169	7.501×10^{-8}	0.4154	−0.1764	1.775×10^{6}	8.237×10^{-4}	4.366×10^{6}
PIF_2-coated SS304	−0.067	4.336×10^{-8}	0.2553	−0.2288	2.207×10^{7}	4.761×10^{-4}	1.543×10^{7}
PIF_4-coated SS304	−0.053	1.097×10^{-8}	0.2769	−0.2369	6.491×10^{7}	1.205×10^{-4}	2.791×10^{7}
$PIFH_1$-coated SS304	−0.144	7.001×10^{-8}	0.2101	−0.2221	2.412×10^{7}	7.688×10^{-4}	4.922×10^{6}
$PIFH_2$-coated SS304	0.112	8.320×10^{-9}	0.2473	−0.1776	3.289×10^{7}	9.136×10^{-5}	2.603×10^{7}
$PIFH_4$-coated SS304	0.222	4.636×10^{-9}	0.3940	−0.2341	5.403×10^{7}	5.091×10^{-5}	2.921×10^{7}

($x \geq 2$) arose from the low-surface-energy CF_2 and CF_3 units on the surfaces of the silylated fluoro-organosilicasol.Fig. 8 presents our proposed representation of the molecular phenomena behind this behavior. After F8261 had bonded onto the DMAc-ST surfaces, the residual SiOH groups forced the perfluoroalkyl chains to coil around the surface in the polar solvent. After silylation with HMDS, the SiOH groups transformed into much-less-polar $SiOSiMe_3$ groups. The much lower polarity of the environment was favorable to the low-surface-energy perfluoroalkyl chains, which could then stretch away from the particles' surface. Thereby, silylation induced surface group rearrangements such that more CF_2 and CF_3 groups, which have surface energies lower than those of methyl groups, were detected on the outer surfaces, corresponding to an increase in the number of F atoms.

3.5. Anticorrosion measurement

So far, the roughness and chemical factors controlling hydrophobicity tuning mechanisms have been verified, Fully covering the surface with silylated fluoro-organosilicasol could achieve stable water repellency. To further examine the corrosion behaviors, potentiodynamic polarization measurements were carried out on SS304, PI-coated SS304, PI-F_x-coated SS304, and PI-FH_x-coated SS304 and the results are shown in Fig. 9 and Table 6 for comparison. Fig. 9 shows the Tafel plots of uncoated/coated SS304 samples. The parameters obtained from polarization measurements such as corrosion potential (E_{corr}), corrosion current density (i_{corr}), polarization resistance (R_p), corrosion rate, anodic and cathodic Tafel slope (β_a and β_c) are given in Table 6. After coating a PI film, E_{corr} increased to −0.191 V from −0.22 V for bare SS304 substrate. According to Table 6, E_{corr} became more positive by spray coating of fluoro-organosilicasol on PI-coated SS304 (PI-F_x and PI-FH_x series). We also observed that PI-FH_x-coated SS304 samples exhibited more positive E_{corr} compared to PI-F_x-coated ones. E_{corr} values were gradually improved with increasing the coating amount of fluoro-organosilicasol. For PI-FH_2- and PI-FH_4- coated SS304, E_{corr} became positive as $E_{corr} = 0.112$ V and 0.222 V, respectively. Moreover, a similar trend was observed in i_{corr} and the corrosion rate, which was directly proportional to i_{corr}. Fluoro-organosilicasol coating provided additional protection to PI-coated SS304 and thus I_{corr} and the corrosion rate can be greatly reduced. Both PI-F_x- and PI-FH_x-coated SS304 showed higher R_p than bare and PI-coated SS304, but there was no great difference in R_p between these two series. Accordingly, additional fluoro-organosilicasol-coated PI films already provided dual barrier protection for corrosion, especially for the PI-FH_x series, which were with superhydrophobicity. Since the PI-FH_x series possesses great water repellency, neither water nor chloride ions in the medium can readily penetrate these dual coatings on SS304. PI-F_x series, which were somehow more sticky to water, thus showed poorer anticorrosion performance (lower E_{corr}) than PI-FH_x series.

The Bode plots obtained from EIS measurement showed in Fig. 9 (b and c) and the impedance modulus |Z| at 0.01hz were also labeled in Table 6. According to Fig. 9(b) and Table 6, PI coating increases the |Z| values and after additional spray coating of fluoro-organosilicasol, |Z| of PI-F_4 and PI-FH_4 both showed almost two orders of magnitude higher than that of bare SS304 and one order of magnitude higher than that of PI-coated SS304. We also used two equivalent circuit models in Fig. 9 (d and e) to described the corrosion process [37]. In these equivalent circuit models, impedance depends on solution resistance (R_s), coating pore resistance (R_{po}), charge transfer resistance (R_{ct}) and constant phase element (CPE), which is better describing behavior of coatings having heterogeneities of structures [37,38]. The graph of the phase angle versus frequency, Fig. 9(c), indicated that for SS304, there was one time constant at around 1 Hz, which is characterized by the equivalent circuit model in Fig. 9(d). For composite coating as PI-F_x and PI-FH_x-coated SS304 here, two time constants can be observed and described as the equivalent circuit model in Fig. 9(e). High frequency time constant, at around 10^3 ~ 10^4 Hz, is related to outer fluoro-organosilicasol coating sprayed on PI coating. Another time constant at low frequency, at around 0.1 ~ 1 Hz, is slightly lower than that of SS304. This might arise from the dual barrier protection of fluoro-organosilicasol-coated-PI surface which further suppress the penetration of the salt water to SS304 surface. The difference in hydrophobicity between PI-F_x and PI-FH_x seemed not to cause major difference in Bode plots except for specimens taking one spray cycle, which revealed that hydrophobicity factor might majorly influenced |Z| values as the PI was not fully covered by layer of particles.In the cross-cut test, PI coating showed good adhesion toward SS304. Even after 7 days immersion in salt water, PI coating adhered well as no pieces were removed by tape, showing in Fig. 9(d). For specimens underwent additional spray coating, 2 % area (2 out of 100 pieces) were removed for PI-FH_4-coated SS304. The removed area increased to 7% for PI-FH_4-coated SS304 soaked in salt water for 7 days as Fig. 9(d) showed. The cross-cut test indicates that spray coating somewhat weakened PI adhesion and need to be operated carefully during preparation.

4. Conclusion

We have successfully prepared superhydrophobic flexible PI hybrid coating on SS304 and determined the mechanism behind superhydrophobicity. Through a simple coating with fluoro-organosilicasol, the obtained PI-F_x hybrid film surfaces that displayed hydrophobicity superior to that of the pristine PI. After modifying the fluoro-organosilicasol through silylation with HMDS, the hydrophilic OH groups were transformed into hydrophobic $OSiMe_3$ groups and the resulting surface-modified PI-FH_x hybrid films were superhydrophobic with low contact angle hysteresis. SEM and AFM imaging revealed particles densely covering the PI surfaces and overlapping to form larger clusters and rougher surfaces, rendering more spaces for air at the interfaces between the water droplets and the material surfaces. ESCA and FTIR spectroscopic data also indicated that after HMDS-mediated silylation of the fluoro-organosilicasol, the depletion of the abundant OH groups led to more CF_2 groups stretching out on the PI surface, which, therefore, became superhydrophobic. The combination of both a rough topology and hydrophobic modification created the superhydrophobic PI surfaces. In corrosion measurement, we observed that PI-F_x and PI-FH_x hybrid coatings both possessed better corrosion protection than SS304 with pristine PI coating and bare metal. We inferred that this performance enhancement

arose from the dual barrier effect of the combination of fluoro-organosilicasol and the PI matrix. Furthermore, silylated fluoro-organosilicasol provided superhydrophobicity, which could repel the corrosive ions (i.e., Cl^-) in the medium, and avoided the possibility of pitting corrosion. From our observation, we believed that superhydrophobicity was a critical factor in E_{corr} in the comparison between PI-F_x and PI-FH_x, pointing out the importance of water repellency. We believe that this technique is feasible and effective in the preparation of superhydrophobic organic hybrid coatings for anticorrosion and also has great potential application in the modification of the properties of other polymers.

Acknowledgment

This project was supported by the Ministry of Science and Technology, Taiwan, under Contract No. NSC 100-2221-E-009-023-MY3 and NSC 102-2221-E-009-175-MY3.

References

[1] M.H. Tsai, Y.C. Huang, I.H. Tseng, H.P. Yu, Y.K. Lin, J. Appl. Polym. Sci. 126 (2012) 365–370.
[2] L. Feng, J.O. Iroh, Prog. Org. Coat. 77 (2014) 590–599.
[3] M.D. Damaceanu, C.P. Constantin, A. Nicolescu, M. Bruma, N. Belomoina, R.S. Begunov, Eur. Polym. J. 50 (2014) 200–213.
[4] A. Nakajima, H. Kazuhito, W. Toshiya, Monash. Chem./Chem. Monthly 132 (2001) 31–41.
[5] D. Quéré, Annu. Rev. Mater. Res. 38 (2008) 71–99.
[6] X. Wang, D. Bin, Y. Jianyong, W. Moran, Nano Today 6 (2011) 510–530.
[7] L. Liu, X. Feiyan, M. Lin, J. Phys. Chem. C 116 (2012) 18722–18727.
[8] G. Scheen, K. Ziouche, Z. Bougrioua, P. Godts, D. Leclercq, T. Lasri, Langmuir 27 (2011) 6490–6495.
[9] Y. Kwon, N. Patankar, J. Choi, J. Lee, Langmuir 25 (2009) 6129–6136.
[10] A. Borras, A. Barranco, A.R. Gonzalez-Elipe, Langmuir 24 (2008) 8021–8026.
[11] Y. Miyahara, K. Mitamura, N. Saito, O. Takai, J. Vac. Sci. Technol. A 27 (2009) 1183–1187.
[12] P.S. Brown, E.L. Talbot, T.J. Wood, C.D. Bain, J.P.S. Badyal, Langmuir 28 (2012) 13712–13719.
[13] T. Furuta, T. Isobe, M. Sakai, S. Matsushita, A. Nakajima, Appl. Surf. Sci. 258 (2012) 2378–2383.
[14] C.S. Sharma, K. Abhishek, H. Katepalli, A. Sharma, Ind. Eng. Chem. Res. 50 (2011) 13012–13020.
[15] Q.F. Xu, B. Mondal, A.M. Lyons, ACS Appl. Mater. Interfaces 3 (2011) 3508–3514.
[16] T. Darmanin, F. Guittard, J. Am. Chem. Soc. 133 (2011) 15627–15634.
[17] B.J. Privett, J. Youn, S.A. Hong, J. Lee, J. Han, J.H. Shin, M. Schoenfisch, Langmuir 27 (2011) 9597–9601.
[18] R.V. Lakshmi, T. Bharathidasan, B.J. Basu, Appl. Surf. Sci. 257 (2011) 10421–10426.
[19] A. Razmjou, E. Arifin, G. Dong, J. Mansouri, V. Chen, J. Membr. Sci. 415–416 (2012) 850–863.
[20] H. Yang, Y. Cheng, F. Xiao, Appl. Surf. Sci. 258 (2011) 1572–1580.
[21] T.J. Athauda, W. Williams, K.P. Roberts, R.R. Ozer, J. Mater. Sci. 48 (2013) 6115–6120.
[22] D. Ebert, B. Bhushan, Langmuir 28 (2012) 11391–11399.
[23] R.G. Karunakaran, C.H. Lu, Z. Zhang, S. Yang, Langmuir 27 (2011) 4594–4602.
[24] L. Xu, J. He, Langmuir 28 (2012) 7512–7518.
[25] Z. He, M. Ma, X. Xu, J. Wang, F. Chen, H. Deng, K. Wang, Q. Zhang, Q. Fu, Appl. Surf. Sci. 258 (2012) 2544–2550.
[26] D. Goswami, S.K. Medda, G. De, ACS Appl. Mater. Interfaces 3 (2011) 3440–3447.
[27] L. Xu, R.G. Karunakaran, J. Guo, S. Yang, ACS Appl. Mater. Interfaces 4 (2012) 1118–1125.
[28] Y. Zhao, M. Li, Q. Lu, Z. Shi, Langmuir 24 (2008) 12651–12657.
[29] W.A. Zisman, Adv. Chem. Ser. 43 (1964) 1–51.
[30] S.D. Wang, S.S. Luo, Appl. Surf. Sci. 258 (2012) 5443–5450.
[31] G. Gong, J. Wu, J. Liu, N. Sun, Y. Zhao, L. Jiang, J. Mater. Chem. 22 (2012) 8257–8262.
[32] H.Y. Gu, Z.Y. Qi, W. Wu, Y. Zeng, L.X. Song, Express Polym. Lett. 8 (2014) 588–595.
[33] K.C. Chang, H.I. Lu, C.W. Peng, M.C. Lai, S.C. Hsu, M.H. Hsu, Y.K. Tsai, C.H. Chang, W.I. Hung, Y. Wei, J.M. Yeh, ACS Appl. Mater. Interfaces 5 (2013) 1460–1467.
[34] N.A. Patankar, Langmuir 26 (2010) 7498–7503.
[35] N. Saleema, D.K. Sarkar, D. Gallant, R.W. Paynter, X.G. Chen, ACS Appl. Mater. Interfaces 3 (2011) 4775–4781.
[36] J. Zuo, P. Keil, M. Valtiner, P. Thissen, G. Grundmeier, Surf. Sci. 602 (2008) 3750–3759.
[37] E. Huttunen-Saarivirtaa, V.E. Yudinb, L.A. Myagkovab, V.M. Svetlichnyi, Prog. Org. Coat. 72 (2011) 269–278.
[38] S.V. Gnedenkova, S.L. Sinebryukhova, V.S. Egorkina, D.V. Mashtalyara, D.A. Alpysbaevab, L.B. Boinovichb, Colloids Surf. A Physicochem. Eng. Asp. 383 (2011) 61–66.